



Volume preserving mesh parameterization based on optimal mass transportation

Kehua Su^a, Wei Chen^b, Na Lei^{c,d,*}, Junwei Zhang^b, Kun Qian^e, Xianfeng Gu^b

^a State Key Laboratory of Software Engineering, Wuhan University, Wuhan, 430072, China

^b Computer Science Department, Stony Brook University, Stony Brook, NY, 11794, USA

^c School of Software, Dalian University of Technology, Dalian, 116620, China

^d Yau Mathematics Science Center, Tsinghua University, Beijing, 100084, China

^e School of Civil Engineering and Mechanics, Kunming University of Science and Technology, Kunming, China

ARTICLE INFO

Keywords:

Parameterization

Volume preserving

Harmonic map

Optimal mass transportation

ABSTRACT

In order to convert a finite element mesh model to the spline representation for the purpose of isogeometric analysis, one needs to parameterize the solid. This work introduces a novel volumetric parameterization method, which guarantees to be free of volume distortion.

Given a simply connected tetrahedral mesh with a single boundary surface, we first compute a harmonic map from the boundary triangle mesh to the unit sphere by non-linear heat diffusion method; then we use the surface harmonic map as the boundary condition to compute the volumetric harmonic map to parameterize the solid onto the unit solid ball; finally we compute an optimal mass transportation map from the unit solid ball with the push-forward volume element induced by the harmonic map onto itself with the Euclidean volume element. The composition of the volumetric harmonic map and the optimal mass transportation map gives an volume-preserving parameterization.

The method has solid theoretic foundation, and is based on conventional algorithms in computational geometry, easy to implement. We have thoroughly tested our algorithm on many solid models in reality. The experimental results demonstrate the efficiency and efficacy of the proposed method. To the best of our knowledge, it is the first work addressing volume-preserving parameterization in the literature.

© 2016 Elsevier Ltd. All rights reserved.

1. Introduction

Recent years have witnessed the rapid development of the methodology of isogeometric analysis [1,2]. In Computer Aided Design (CAD) field, the geometric shapes are represented as Spline surfaces/solids. In Computer Aided Engineering (CAE) field, the isoparametric philosophy represents the solution space for dependent variables in terms of the same functions which represent the geometry. In reverse engineering field [3], shapes in real life are often acquired by 3D scanning technologies and represented as point clouds. The point cloud is triangulated to generate the boundary surface, the tetrahedron mesh is generated to tessellate the interior using automatic meshing generation tools, such as Tetgen [4].

In order to apply isogeometric analysis method, the solid needs to be parameterized and fit by volumetric Splines.

Volumetric mesh parameterization refers to the process of mapping a tetrahedral mesh onto a canonical domain in three dimensional Euclidean space \mathbb{R}^3 . The parameterization unavoidably introduces geometric distortions. Geometric distortions can be classified into two categories: angle distortion and volume distortion. A parameterization preserves both angle and volume element must be isometric, hence preserves curvatures. In general, isometric parameterization doesn't exist between the input volume and the Euclidean domain, therefore people pursue either angle-preserving parameterization or volume-preserving parameterization.

Volumetric angle-preserving parameterization can be approximated by volumetric harmonic mapping. Intuitively, the harmonic energy of a map between two Riemannian manifolds measures the elastic deformation energy induced by the map, a harmonic map minimizes the harmonic energy. In surface case, a harmonic map between two genus zero closed surfaces must be angle-preserving

* Corresponding author at: School of Software, Dalian University of Technology, Dalian, 116620, China.

E-mail addresses: skh@whu.edu.cn (K. Su), nalei@outlook.com (N. Lei), junwei.zhang@stonybrook.edu (J. Zhang), gu@cs.stonybrook.edu (X. Gu).

(conformal). Finding harmonic maps between manifolds is equivalent to solve special geometric partial differential equations. For surface case, the necessary and sufficient condition for a map to be harmonic is that the tangential component of the Laplacian at each point is zero; for volume case, a map is harmonic if the Laplacian is zero everywhere in the interior. In discrete settings, these geometric PDEs can be solved approximately using finite element method.

Locally, angle-preserving parameterization can be treated as scaling transformations, therefore preserves local shapes. But angle-preserving parameterization may induce large volume distortions. For surface case, if a long tube surface is conformally mapped onto the planar disk, the area distortion at the tip is exponential with respect to the height of the tube. Large volume distortions will introduce numerical inaccuracy/instability for the downstream geometric processing tasks. For example, in volumetric spline fitting, the geometric approximation accuracy in the region with large volume distortions is low, or complicated knot structure is required to compensate the large distortions. In practice, for some special applications, volume-preserving parameterizations have advantages.

To the best of our knowledge, there are few works for volume-preserving parameterization. In the current work, we propose to use optimal mass transportation framework to achieve this goal. Given a convex domain in the Euclidean space with two different measures (volume elements), the optimal transportation map is an automorphism of the domain itself, which transforms the source measure to the target measure in the most economic way. According to Brenier's theorem, the optimal transportation map is the gradient map of a convex function defined on the domain. The problem of finding the optimal transportation map boils down to finding the convex function. In practice, the target measure is approximated by discrete measures (Dirac measures), the convex function is approximated by the upper envelope of a family of hyper-planes in \mathbb{R}^4 , the normals of the planes are fixed but the heights (intercepts) are unknown. The heights can be obtained by optimizing a convex energy using Newton's method.

In our current work, for a given simply connected tetrahedral mesh with a single boundary surface, we first map it onto the unit solid ball using a harmonic map, and the volume element of the initial mesh is pushed forward to the unit ball; then we compute an optimal mass transportation map of the unit ball from the push-forward volume element to the canonical Euclidean volume element. The composition of the harmonic map and the optimal mass transportation map gives the volume-preserving parameterization of the initial tetrahedral mesh.

Contributions. This work proposes a novel algorithm to compute volume-preserving parameterization for a simply connected tetrahedral mesh with a single boundary surface. The algorithm is based on the discrete optimal mass transportation theory, therefore is rigorous. To the best of our knowledge, this is the first work on volume-preserving tetrahedral mesh parameterization.

2. Previous works

The literature for parameterization is vast, a thorough survey is beyond the scope of the current work. In the following, we only briefly review the most related works in volumetric parameterization and optimal mass transportation.

2.1. Volumetric parameterization

There are mainly three kinds of methods for volumetric parameterization.

The most widely used method is harmonic mapping, which is first proposed by Wang et al. in [5]. They use a variational

procedure to reduce the discrete harmonic energy and map a genus-zero volume to a solid sphere, and later used this method on brain mapping [6]. Li et al. [7] use a meshless approach to compute the harmonic mapping between two solid models. Xu et al. [8] compute a bi-harmonic map applying a multiple fundamental solutions system for fast computation. Martin et al. construct trivariate spline for cylindrical volumes by computing harmonic volumetric parameterization in [9]. Xia et al. [10] parameterize star-shaped volumes by Green's functions. They show that the constructed map is bijective and smooth except at the unique critical point. They also propose an algorithm to decompose a volume into the direct product of a two-dimensional (2D) surface and a one-dimensional (1D) curve and then trace the integral curve along the harmonic function in [11]. Gupta et al. [12] present an approach for the problem of volumetric parameterization of a general nonconvex (genus-0) domain to its topologically equivalent convex domain by combining harmonic map and streamline approach.

Many mappings are constructed by means of generalized barycentric coordinates with closed form expressions [13]. The mean-value coordinates method was extended from surface [14] to volume by Ju et al. [15] and Floater et al. [16] to compute the interpolation of volumetric data. Lipman et al. [17] propose Green coordinates which lead to mappings with shape-preserving property.

Another kind of popular method is to find a mapping which minimizes a specific energy. Chao et al. [18] minimize the so-called ARAP (as-rigid-as-possible) deformation energy, which is a simple geometric model measuring distance from the Jacobian of the mapping to an isometry. Frame field driven methods use the energy measuring difference between the Jacobian and the guidance frame field [19–21] and compute the volumetric parameterization in a variational way. Jin et al. [22] extend the stretch-minimizing method to volumetric parameterization by deriving a 3D version of stretch-distortion energy and incorporating fixed boundary conditions.

2.2. Optimal mass transportation

Monge raised the classical *Optimal Mass Transport Problem* that concerns determining the optimal way, with minimal transportation cost, to move a pile of soil from one place to another [23]. Kantorovich [24] has proved the existence and uniqueness of the optimal transport plan based on linear programming. Monge–Kantorovich optimization has been used in numerous fields from physics, econometrics to computer science including data compression and image processing [25]. Recently, researchers have realized that optimal transport could provide a powerful tool in image processing, if one could reduce its high computational cost [26,27]. However, it has one fundamental disadvantage that the number of variables is $O(n^2)$, which is unacceptable to computer vision and medical imaging applications since a high resolution 3D surface normally includes up to hundreds of thousands of vertices.

An alternative Monge–Brenier optimization scheme can significantly reduce the number of variables to be optimized. In late 1980's, Brenier [28] developed a different approach for a special class of optimal transport problems, where the cost function is a quadratic distance. Brenier's theory shows that the optimal transport map is the gradient map of a special convex function. Assume the target domain is discretized to n samples, the Monge–Brenier's approach reduces the unknown variables from $O(n^2)$ to $O(n)$, which greatly reduces the computation cost, and improves the efficiency. In our framework, we take Monge–Brenier's approach. However, our work is based on the newly discovered variational principle [29] which is the underpinning of Monge–Brenier's approach. Our framework is general and works with any valid measures, μ and ν , defined on two volumes. Within the scope of

this paper, we only consider the volume induced measures. Recently, Su et al. applied Brenier's approach for shape matching and comparison in computer vision field [30]. Similar method has been used for surface area-preserving parameterization in graphics/visualization field by Kaufman et al. in [31]. So far, to the best of the authors' knowledge, there is no existing work on volume-preserving parameterization.

3. Theoretic background

This section briefly introduces the theoretic background of harmonic mapping and Optimal Mass Transport theory. We refer readers to classical textbooks [32,33] for harmonic map, the seminal papers [24] on optimal transport map with Kantorovich's method, [28,34] for Brenier's approach, [29] for more detailed proofs of the proposed method.

3.1. Harmonic maps

Smooth harmonic map theory can be found in [32]. This section focuses on discrete harmonic maps (see Fig. 1). We use K to represent the simplicial complex, u, v to denote the vertices, and $\{u, v\}$ to denote the edge spanned by u, v . We use f, g to represent the piecewise linear functions defined on K , and use \mathbf{g} to represent vector valued functions. We use Δ_{PL} to represent the discrete Laplace–Beltrami operator.

Definition 3.1. All piecewise linear functions defined on K form a linear space, denoted by $C^{PL}(K)$.

Definition 3.2. Suppose a set of string constants $k_{u,v}$ are assigned for each edge $\{u, v\}$, the inner product on C^{PL} is defined as the quadratic form

$$\langle f, g \rangle = \frac{1}{2} \sum_{\{u,v\} \in K} k_{u,v} (f(u) - f(v))(g(u) - g(v)). \quad (1)$$

The harmonic energy is defined as the norm on C^{PL} .

Definition 3.3 (Harmonic Energy). Suppose $f \in C^{PL}$, the string energy is defined as

$$E(f) = \langle f, f \rangle = \frac{1}{2} \sum_{\{u,v\} \in K} k_{u,v} \|f(u) - f(v)\|^2. \quad (2)$$

Definition 3.4 (Laplace–Beltrami Operator). The piecewise Laplace–Beltrami operator is the linear operator $\Delta_{PL} : C^{PL} \rightarrow C^{PL}$ on the space of piecewise linear functions of K , defined by the formula

$$\Delta_{PL}f(u) := \sum_{\{u,v\} \in K} k_{u,v} (f(v) - f(u)). \quad (3)$$

Surface case. Suppose (S, \mathbf{g}) is a smooth Riemannian surface embedded in \mathbb{R}^3 , \mathbf{g} is the induced Euclidean metric. One can put the sample points on the smooth surface, compute a geodesic triangulation using these sample points as vertices, then replace each triangle on the surface by a Euclidean triangle fixing the vertex positions. In this way, we obtain a simplicial complex, a piecewise linear surface, denoted as K .

Suppose $\{u, v\}$ is an edge on K , shared by two faces $\{u, v, w\}, \{l, v, u\}$, then we can define the edge weight as

$$k_{u,v} = \cot \theta_{u,v}^w + \cot \theta_{v,u}^l, \quad (4)$$

where $\theta_{u,v}^w$ is the corner angle at the vertex w in the triangle $\{u, v, w\}$, $\theta_{v,u}^l$ the corner angle at the vertex l in the triangle $\{v, u, l\}$

respectively. Let $\mathbf{f} : K \rightarrow \mathbb{S}^2$ be a mapping, represented by channel scalar functions (f^1, f^2, f^3) , then its Laplace–Beltrami operator is

$$\Delta_{PL}\mathbf{f} = (\Delta_{PL}f^1, \Delta_{PL}f^2, \Delta_{PL}f^3), \quad (5)$$

its normal component is given by

$$\Delta_{PL}\mathbf{f}^\perp = \Delta_{PL}\mathbf{f} - \langle \Delta_{PL}\mathbf{f}, \mathbf{f} \rangle \mathbf{f}, \quad (6)$$

its tangential component is

$$\Delta_{PL}\mathbf{f}^\parallel = \Delta_{PL}\mathbf{f} - \Delta_{PL}\mathbf{f}^\perp. \quad (7)$$

The mapping is discrete harmonic, if and only if for each vertex $u \in K$, the tangential component vanishes

$$\Delta_{PL}\mathbf{f}^\parallel(u) = 0, \quad \forall u \in K. \quad (8)$$

Volume case. Suppose (M, \mathbf{g}) is a solid embedded in \mathbb{R}^3 , where \mathbf{g} is the induced Euclidean metric. We put sample points on both the boundary surface and the interior of the solid, then compute a triangulation using the samples as vertices, denote the simplicial complex as K .

Suppose $\{u, v\}$ is an edge in K , its length is $l_{u,v}$, and $\{u, v, w, t\}$ is a tetrahedron attaching to the edge $\{u, v\}$, the dihedral angle in the tetrahedron on edge $\{w, t\}$ is $\theta_{u,v}^{w,t}$, the edge weight is defined as

$$k_{u,v} = \frac{1}{12} \sum_{w,t} l_{u,v} \cot \theta_{u,v}^{w,t}. \quad (9)$$

Let $\mathbf{f} : K \rightarrow \mathbb{D}^3$ be a mapping from the simplicial complex K to the unit solid ball $\mathbb{D}^3 \subset \mathbb{R}^3$, its Laplacian is

$$\Delta_{PL}\mathbf{f}(u) = \sum_v k_{u,v} (\mathbf{f}(v) - \mathbf{f}(u)). \quad (10)$$

We fix the boundary mapping $\mathbf{f}|_{\partial K} : \partial K \rightarrow \mathbb{S}^2$, if the mapping is harmonic with Dirichlet boundary condition, then for all interior vertex, its Laplacian vanishes,

$$\Delta_{PL}\mathbf{f}(u) = 0, \quad \forall u \notin \partial K. \quad (11)$$

3.2. Optimal mass transport

Monge [23] raised the optimal mass transportation problem in the 18th century.

Problem 3.1 (Optimal Mass Transport). Suppose $(X, \mu), (Y, \nu)$ are metric spaces with probabilities measures, which has the same total mass $\int_X \mu dx = \int_Y \nu dy$. A map $T : X \rightarrow Y$ is *measure preserving*, if for any measurable set $B \subset Y$, $\mu(T^{-1}(B)) = \nu(B)$. Given a transportation cost function $c : X \times Y \rightarrow \mathbb{R}$, find the measure preserving map $T : X \rightarrow Y$ that minimizes the total transportation cost

$$\mathcal{C}(T) := \int_X c(x, T(x)) d\mu(x). \quad (12)$$

In the 1940s, Kantorovich introduced the relaxation of Monge's problem and solved it using linear programming method [24].

At the end of 1980's, Brenier [28] discovered the intrinsic connection between optimal mass transport map and convex geometry.

Definition 3.5 (Convex Function). Suppose $f : X \rightarrow \mathbb{R}$ is a function, f is convex if $f\left(\frac{x_1+x_2}{2}\right) \leq \frac{1}{2}(f(x_1) + f(x_2))$. If f is C^2 continuous convex function, its Hessian matrix is semi-positive definite. $\left(\frac{\partial^2 f}{\partial x_i \partial x_j}\right) \geq 0$.



Fig. 1. The bimba surface is conformally mapped onto the unit sphere. The mapping is unique up to a Möbius transformation.

Definition 3.6 (Gradient Map). Suppose $f : X \rightarrow \mathbb{R}$ is a function, the gradient map $\nabla f : X \rightarrow Y$ is defined as $x \mapsto \nabla f(x)$.

Theorem 3.1 (Brenier). Suppose X and Y are the Euclidean space \mathbb{R}^n , and the transportation cost is the quadratic Euclidean distance $c(x, y) = |x - y|^2$. If μ is absolutely continuous and μ and ν have finite second order moments, then there exists a convex function $f : X \rightarrow \mathbb{R}$, its gradient map ∇f gives the solution to the Monge's problem. Furthermore, the optimal mass transportation map is unique.

This theorem converts the Monge's problem to solving the following Monge–Amperé partial differential equation:

$$\det \left(\frac{\partial^2 f(x)}{\partial x_i \partial x_j} \right) = \frac{\mu(x)}{\nu \circ \nabla f(x)}.$$

Detailed proof can be found in [35].

3.3. Discrete optimal mass transport

We focus on the Brenier's approach, as illustrated in Fig. 2. Suppose μ has compact support on X , define $\Omega = \text{supp } \mu = \{x \in X | \mu(x) > 0\}$, assume Ω is a convex domain in X . The space Y is discretized to $Y = \{y_1, y_2, \dots, y_k\}$ with Dirac measure $\nu = \sum_{j=1}^k v_j \delta(y - y_j)$ (see Fig. 2).

We define a height vector $\mathbf{h} = (h_1, h_2, \dots, h_n) \in \mathbb{R}^k$, consisting of k real numbers. For each $y_i \in Y$, we construct a hyperplane defined on X ,

$$\pi_i(\mathbf{h}) : \langle x, y_i \rangle + h_i = 0. \quad (13)$$

Define a function

$$u_{\mathbf{h}}(x) = \max_{i=1}^k \{\langle x, y_i \rangle + h_i\}, \quad (14)$$

then $u_{\mathbf{h}}(x)$ is a convex function. We denote its graph by $G(\mathbf{h})$, which is an infinite convex polyhedron with supporting planes $\pi_i(\mathbf{h})$. The projection of $G(\mathbf{h})$ induces a polygonal partition of Ω ,

$$\Omega = \bigcup_{i=1}^k W_i(\mathbf{h}), \quad (15)$$

where each cell $W_i(\mathbf{h})$ is the projection of a facet of the convex polyhedron $G(\mathbf{h})$ onto Ω ,

$$W_i(\mathbf{h}) = \{x \in X | u_{\mathbf{h}}(x) = \langle x, y_i \rangle + h_i\} \cap \Omega. \quad (16)$$

Note that, this partition is similar to the power diagram concept in computational geometry [36]. The volume of $W_i(\mathbf{h})$ is given by

$$w_i(\mathbf{h}) = \int_{W_i(\mathbf{h})} \mu(x) dx. \quad (17)$$

The convex function $u_{\mathbf{h}}$ on each cell $W_i(\mathbf{h})$ is a linear function $\pi_i(\mathbf{h})$, therefore, the gradient map

$$\text{grad } u_{\mathbf{h}} : W_i(\mathbf{h}) \rightarrow y_i, \quad i = 1, 2, \dots, k \quad (18)$$

maps each $W_i(\mathbf{h})$ to a single point y_i .

The following theorem plays a fundamental role for discrete optimal mass transport theory,

Theorem 3.2. For any given measure ν , such that $\sum_{j=1}^n v_j = \int_{\Omega} \mu$, $v_j > 0$, there must exist a height vector \mathbf{h} unique up to adding

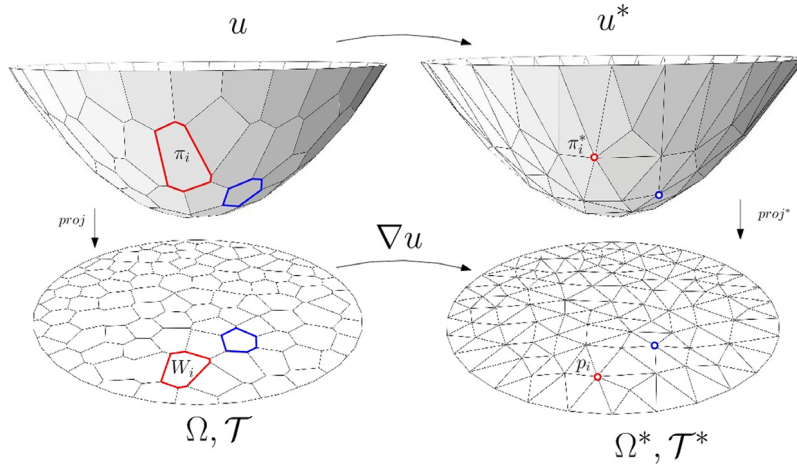


Fig. 2. Discrete optimal mass transportation map with Brenier's approach.

a constant vector (c, c, \dots, c) , the convex function Eq. (14) induces the cell decomposition of Ω , Eq. (15), such that the following volume-preserving constraints are satisfied for all cells,

$$\int_{W_i(\mathbf{h})} \mu(x) dx = v_i, \quad i = 1, 2, \dots, n. \quad (19)$$

Furthermore, the gradient map $\text{grad } u_{\mathbf{h}}$ optimizes the following transportation cost

$$C(T) := \int_{\Omega} |x - T(x)|^2 \mu(x) dx. \quad (20)$$

The existence and uniqueness was first proven by Alexandrov [37] using a topological method; the existence was also proven by Aurenhammer [38], the uniqueness and optimality was proven by Brenier [28]. Recently, Gu et al. [29] give a novel proof for the existence and uniqueness based on the variational principle, which leads to the computational algorithm directly.

Define the admissible space of height vectors $H_0 := \{\mathbf{h} | \sum_{j=1}^k h_j = 0 \text{ and } \int_{W_i(\mathbf{h})} \mu > 0, \forall i = 1, \dots, k\}$. Then define the energy $E(\mathbf{h})$,

$$E(\mathbf{h}) = \int_{\Omega} u_{\mathbf{h}}(x) \mu(x) dx - \sum_{i=1}^k v_i h_i \quad (21)$$

or equivalently

$$E(\mathbf{h}) = \int_{\Omega} \sum_{i=1}^k w_i(\eta) d\eta_i - \sum_{i=1}^k v_i h_i + C, \quad (22)$$

where C is a constant. Consider the shape bounded by the graph $G(\mathbf{h})$, the horizontal plane $\{x_{n+1} = 0\}$ and the cylinder consisting of vertical lines through $\partial\Omega$, the volume of the shape is given by the first term.

The gradient of the energy is given by

$$\nabla E(\mathbf{h}) = (w_1(\mathbf{h}) - v_1, \dots, w_k(\mathbf{h}) - v_k)^T. \quad (23)$$

Suppose the cells $W_i(\mathbf{h})$ and $W_j(\mathbf{h})$ intersect at a cell $e_{ij} = W_i(\mathbf{h}) \cap W_j(\mathbf{h}) \cap \Omega$, then the Hessian of $E(\mathbf{h})$ is given by

$$\frac{\partial^2 E(\mathbf{h})}{\partial h_i \partial h_j} = \begin{cases} \frac{\int_{e_{ij}} \mu(x) dx}{|y_j - y_i|} & W_i(\mathbf{h}) \cap W_j(\mathbf{h}) \cap \Omega \neq \emptyset \\ 0 & \text{otherwise.} \end{cases} \quad (24)$$

The following theorem lays down the theoretic foundation of our OMT map algorithm.

Theorem 3.3 (Discrete Optimal Mass Transport [29]). If Ω is convex, then the admissible space H_0 is convex, the energy (Eq. (21)) is convex. The unique global minimum \mathbf{h}_0 is an interior point of H_0 . Furthermore, the gradient map (Eq. (18)) induced by the minimum \mathbf{h}_0 is the unique optimal mass transport map, which minimizes the total transportation cost (Eq. (20)).

The proof of Theorem 3.3 is reported in [29]. Due to the convexity of the volume energy Eq. (21), With this theory, the global minimum can be obtained efficiently using Newton's method. Comparing to Kantorovich's approach, where there are $O(n^2)$ unknowns, this approach has only $O(n)$ unknowns.

The optimal mass transportation theory holds for arbitrary dimensions. In practice, there are key differences between surface and volume cases. OMT requires the source domain to be convex. For surface case (see Fig. 3), it is easy to parameterize a simply connected surface with a single boundary to a convex planar domain, such as using harmonic map or conformal map; in contrast, this is much more challenging for volume case, because volumetric harmonic map may not be homeomorphic. Therefore, the preprocessing step of volume OMT is much more complicated and challenging.

4. Computational algorithms

This section focuses on the algorithms. The theoretic deduction for spherical harmonic map can be found in [39], for volumetric harmonic map in [5], for optimal mass transportation map in [30]. In order to be complete, we give all details of these algorithms.

4.1. Spherical harmonic maps

Suppose K is a triangle mesh (a triangulated polyhedral surface), the following algorithm finds a harmonic map from the mesh to the unit sphere $\mathbf{f} : K \rightarrow \mathbb{S}^2$. The input to the algorithm is a genus zero closed triangle mesh K , and a step length parameter δ , a threshold ε . The algorithm is summarized in Alg. 1.

Step 1. Initial map We construct the Gauss map as the initial map. For each face $\{u, v, w\}$, we compute the area of the face,

$$a_{u,v,w} = \frac{1}{2} |(v - u) \times (w - u)|,$$

and the normal to the face,

$$\mathbf{n}_{u,v,w} := \frac{(v - u) \times (w - u)}{2a_{u,v,w}}.$$

Then we compute the normal to each vertex

$$\mathbf{n}_u = \frac{\sum_{v,w} \mathbf{n}_{u,v,w} a_{u,v,w}}{\left| \sum_{v,w} \mathbf{n}_{u,v,w} a_{u,v,w} \right|}.$$

The Gauss map maps each vertex to its normal,

$$\mathbf{G}(u) \leftarrow \mathbf{n}_u.$$

The initial map is set to be the Gauss map.

Step 2. Diffusion We reduce the harmonic energy. For each vertex, we compute its Laplacian $\Delta_{PL}\mathbf{f}(u)$ using formula Eq. (5), project the Laplacian onto the tangent plane using Eq. (7), then we update the image of the mapping of each vertex,

$$\mathbf{f}(u) \leftarrow \mathbf{f}(u) - \delta \Delta_{PL}\mathbf{f}^{\parallel},$$

where δ is a step length parameter.

Step 3. Normalization In order to remove the Möbius ambiguity, we need to enforce the mass center of the image coincides with the origin. For each vertex, we compute the mass associated with it

$$a_u = \frac{1}{3} \sum_{v,w} a_{u,v,w},$$

the center of the mass is given by

$$\mathbf{c} = \frac{\sum_u \mathbf{f}(u) a_u}{\sum_{u,v,w} a_{u,v,w}}.$$

We update the image of each vertex as

$$\mathbf{f}(u) \leftarrow \frac{\mathbf{f}(u) - \mathbf{c}}{\|\mathbf{f}(u) - \mathbf{c}\|}.$$

Step 4. Iteration We repeat step 2 and 3, compute the harmonic energy at each step using Eq. (2). If the difference between the energies of two consecutive steps is less than the threshold ϵ , the algorithm terminates.

Algorithm 1 Spherical Harmonic Map

Input: A genus 0 closed triangle mesh M , a step length parameter δ , a threshold ϵ .

Output: A harmonic map from M to the unit sphere, $\mathbf{f} : M \rightarrow \mathbb{S}^2$.

Compute the Gauss map, $G : M \rightarrow \mathbb{S}^2$, initialize the map $\mathbf{f} \leftarrow G$.
repeat

 Compute the Laplacian of each vertex $\Delta_{PL}\mathbf{f}(u), \forall u \in M$.

 Compute the tangential component of the Laplacian $\Delta_{PL}^{\parallel}\mathbf{f}(u), \forall u \in M$.

 Update the mapping $\mathbf{f}(u) \leftarrow \mathbf{f}(u) - \delta \Delta_{PL}^{\parallel}\mathbf{f}(u), \forall u \in M$.

 Normalize the mapping, such that the center of mass is at the origin.

 Compute the harmonic energy of the current mapping $E(\mathbf{f})$.

until the change of the harmonic energy is less than ϵ .

return The harmonic map $f : M \rightarrow \mathbb{S}^2$.

4.2. Volumetric harmonic map

Suppose M is a tetrahedral mesh embedded in \mathbb{R}^3 , M is simply connected with a single boundary surface, namely a topological solid ball. We would like to map M onto the unit solid ball in \mathbb{R}^3 by a discrete harmonic map $\mathbf{f} : M \rightarrow \mathbb{D}^3$.

Step 1. Boundary map The boundary of M is a triangle mesh ∂M , which is a topological sphere. Similarly, the boundary of the solid ball \mathbb{D}^3 is the unit sphere $\partial \mathbb{D}^3 = \mathbb{S}^2$. We use the algorithm described in the last subsection to find the boundary map $\mathbf{h} : \partial M \rightarrow \mathbb{S}^2$.

Step 2. Interior map The harmonic map $\mathbf{f} : M \rightarrow \mathbb{D}^3$ can be obtained by solving the Laplace equation with the Dirichlet boundary condition,

$$\begin{cases} \Delta_{PL}\mathbf{f}(u) = \mathbf{0}, & \forall u \notin \partial M \\ \mathbf{f}(u) = \mathbf{h}(u), & \forall u \in \partial M \end{cases} \quad (25)$$

for each interior vertex u , the discrete Laplacian of \mathbf{f} at u $\Delta_{PL}\mathbf{f}(u)$ is $\mathbf{0}$, the formulation is given in Eqs. (10) and (11). The discrete Laplace equation is a large sparse linear system, it can be shown that the linear system is positive definite, therefore the solution exists and is unique. In practice, we use conjugate gradient method to solve the linear system, which is stable and efficient.

Algorithm 2 Volumetric Harmonic Map

Input: A simply connected tetrahedral mesh M with a single boundary, a step length parameter δ , a threshold ϵ .

Output: A harmonic map from M to the solid ball, $\mathbf{f} : M \rightarrow \mathbb{D}^3$.

Compute a harmonic map from the boundary surface to the unit sphere, $\mathbf{f} : \partial M \rightarrow \mathbb{S}^2$,

Solve the Laplace equation with the Dirichlet boundary condition Eqn. (25).

return The volumetric harmonic map $f : M \rightarrow \mathbb{D}^3$.

The volumetric harmonic map may not be injective, non-homeomorphic parameterization will cause some problems in IGA solving as shown in the following references [40,41]. We can use local detection and local modification as proposed in [42] to avoid the few flip elements.

4.3. Discrete optimal mass transportation map

Given a discrete point set $P \subset \mathbb{R}^3, P = \{(p_u, A_u), u \in \mathcal{L}\}$, where \mathcal{L} is a index set, such that

$$\sum_{u \in \mathcal{L}} A_u = \frac{4}{3} \pi.$$

Our goal is to find a discrete optimal mass transportation from the unit solid ball to the measured point set P , denoted as $\varphi : \mathbb{D}^3 \rightarrow P$. The algorithm pipeline is summarized in Alg. 3.

Brenier potential. According to Brenier's theorem, there should be a convex function, the so-called Brenier potential $f : \mathbb{D}^3 \rightarrow \mathbb{R}$, the optimal mass transportation map is given by the gradient map of the Brenier potential.

In the discrete setting, the Brenier potential is a piecewise linear convex function, constructed as follows. For each vertex $u \in M$, suppose $\mathbf{f}(u)$ is (a_u, b_u, c_u) , we construct a plane π_u in the four dimensional Euclidean space \mathbb{R}^4 , namely a linear function

$$\pi_u(x, y, z) = a_u x + b_u y + c_u z + h_u.$$

The Brenier potential is defined as

$$f(x, y, z) := \max_{u \in M} \pi_u(x, y, z) = \max_{u \in M} \{a_u x + b_u y + c_u z + h_u\}$$

its graph is the *upper envelope* of family of planes $\{\pi_u, u \in M\}$ in \mathbb{R}^4 .

We use $\Omega(\mathbf{h})$ to represent the (open) convex polyhedron of the upper envelope, where $\mathbf{h} = (h_u)$ is the height vector. π_u 's are the supporting planes of the upper envelope $\Omega(\mathbf{h})$, the face F_u is the intersection between π_u and $\Omega(\mathbf{h})$,

$$F_u = \Omega(\mathbf{h}) \cap \pi_u,$$

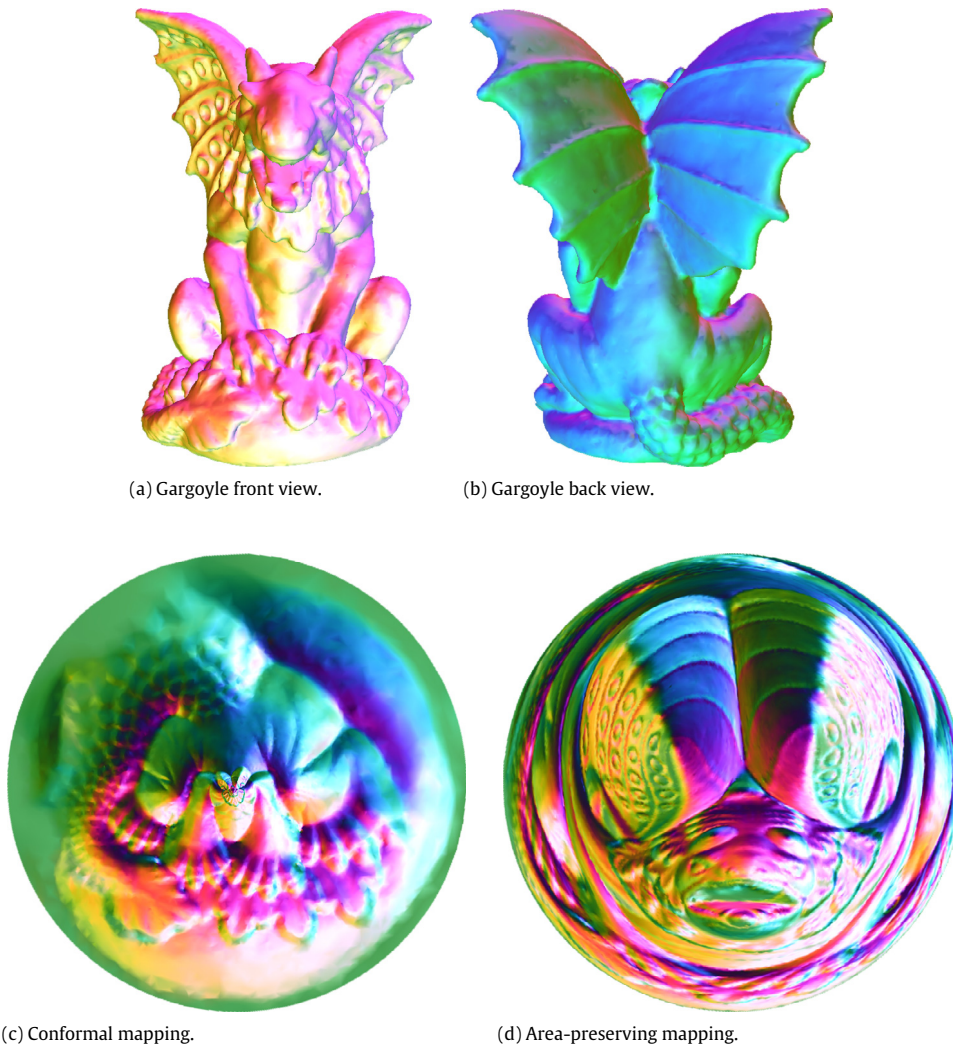


Fig. 3. The gargoyle surface is conformally mapped onto the unit disk (c). The conformal factor is treated as the measure density μ . The optimal transportation map is carried out between the measure density μ and the planar measure density (d), which induces the area-preserving mapping from the surface (a), (b) to the unit disk.

the projection of F_u into \mathbb{R}^3 is defined as a cell W_u in \mathbb{R}^3 ,

$$W_u(\mathbf{h}) := \{(x, y, z) \in \mathbb{R}^3 \mid \nabla f(x, y, z) = (a_u, b_u, c_u)\}$$

therefore, the projection of the upper envelope $\Omega(\mathbf{h})$ to \mathbb{R}^3 induces a cell decomposition of the unit solid ball, denoted as $\mathcal{D}(\mathbf{h})$:

$$\mathbb{D}^3 = \bigcup_{u \in M} \mathbb{D}^3 \cap W_u(\mathbf{h}),$$

we call this cell decomposition as the *power Voronoi diagram* of \mathbb{D}^3 . The volume of each cell is defined as

$$w_u(\mathbf{h}) = \text{vol}(\mathbb{D}^3 \cap W_u(\mathbf{h})).$$

Legendre dual. The computation of the upper envelop of a family of planes $\{\pi_u, u \in M\}$ is converted to convex construction of its Legendre dual.

Definition 4.1 (Legendre Dual). Suppose $f : \mathbb{R}^3 \rightarrow \mathbb{R}$, its Legendre dual is a function $f^* : \mathbb{R}^3 \rightarrow \mathbb{R}$, defined as

$$f^*(x^*, y^*, z^*) := \sup_{(x, y, z) \in \mathbb{R}^3} \{xx^* + yy^* + zz^* - f(x, y, z)\}.$$

Each plane $\pi_u(x, y, z) = a_ux + b_uy + c_uz + h_u$ is dual to a point $\pi_u^* := (a_u, b_u, c_u, -h_u) \in \mathbb{R}^4$.

The upper envelope of the supporting planes

$$\Omega(\mathbf{h}) = \text{Env}(\{\pi_u, u \in M\})$$

is the graph of the Brenier potential f ; the graph of the Legendre dual of the Brenier potential f^* is the lower convex hull of the dual points of the supporting planes

$$\Omega^*(\mathbf{h}) := \text{Conv}(\{\pi_u^*, u \in M\}).$$

The projection of the lower convex hull $\Omega^*(\mathbf{h})$ to \mathbb{R}^3 forms a triangulation, which we call as the *power Delaunay triangulation*, denoted as $\mathcal{T}(\mathbf{h})$.

The dual relations between the power Voronoi diagram $\mathcal{D}(\mathbf{h})$ and the power Delaunay triangulation $\mathcal{T}(\mathbf{h})$ can be represented as follows: each cell $W_u(\mathbf{h}) \subset \mathcal{D}(\mathbf{h})$ is dual to the vertex $\mathbf{f}(u) \subset \mathcal{T}(\mathbf{h})$; the 3 dimensional cell $W_u(\mathbf{h}) \cap W_v(\mathbf{h}) \subset \mathcal{D}(\mathbf{h})$ is dual to the edge $\{\mathbf{f}(u), \mathbf{f}(v)\} \subset \mathcal{T}(\mathbf{h})$; each vertex in the Voronoi diagram is the intersection of 4 cells $W_u(\mathbf{h}) \cap W_v(\mathbf{h}) \cap W_w(\mathbf{h}) \cap W_l(\mathbf{h}) \subset \mathcal{D}(\mathbf{h})$ corresponds to a tetrahedron in the Delaunay triangulation $\{\mathbf{f}(u), \mathbf{f}(v), \mathbf{f}(w), \mathbf{f}(l)\} \subset \mathcal{T}(\mathbf{h})$.

Optimization. The key to solving the optimal mass transportation map is to find the appropriate height vector \mathbf{h} , then construct the upper envelop $\Omega(\mathbf{h})$, and the Brenier potential function, whose gradient map is the desired map. The height vector is the unique

minimizer of the following convex energy

$$E(\mathbf{h}) = \int^{\mathbf{h}} \sum_{u \in M} w_u(\eta) d\eta_u - \sum_{u \in M} A_u h_u,$$

with the constraint

$$\sum_{u \in M} A_u h_u = 0.$$

Due to the convexity of the energy, it can be optimized using Newton's method. The gradient of the energy has the form

$$\nabla E(\mathbf{h}) = (w_u(\mathbf{h}) - A_u), \quad u \in M. \quad (26)$$

The Hessian matrix of the energy is constructed as follows. If the cells $W_u(\mathbf{h})$ and $W_v(\mathbf{h})$ are adjacent in the power Voronoi diagram $\mathcal{D}(\mathbf{h})$, then their intersection is a 2-cell $W_u(\mathbf{h}) \cap W_v(\mathbf{h})$, the dual of this 2-cell in the power Delaunay triangulation $\mathcal{T}(\mathbf{h})$ is an edge $\{\mathbf{f}(u), \mathbf{f}(v)\}$, then we define

$$k_{u,v} := \frac{\text{Area}(W_u(\mathbf{h}) \cap W_v(\mathbf{h}))}{|\mathbf{f}(u) - \mathbf{f}(v)|}.$$

If $W_u(\mathbf{h}) \cap W_v(\mathbf{h}) = \emptyset$, then the corresponding $k_{u,v}$ is 0. The Hessian matrix is given by

$$\frac{\partial^2 E(\mathbf{h})}{\partial h_u \partial h_v} := \begin{cases} -k_{u,v} & u \neq v \\ \sum_w k_{u,w} & u = v. \end{cases} \quad (27)$$

At the first step, we initialize the height vector as

$$h_u = -\frac{1}{2} \langle \mathbf{f}(u), \mathbf{f}(u) \rangle = \frac{1}{2} (a_u^2 + b_u^2 + c_u^2).$$

At each step, we solve the linear system

$$\left(\frac{\partial^2 E(\mathbf{h})}{\partial h_u \partial h_v} \right) \delta \mathbf{h} = \nabla E(\mathbf{h})$$

then update the height vector $\mathbf{h} \leftarrow \mathbf{h} - \delta \mathbf{h}$, until the norm of the gradient $\nabla E(\mathbf{h})$ is less than a predefined threshold.

Algorithm 3 Optimal Mass Transport Map (OMT-Map)

Input: A discrete point set in \mathbb{R}^3 with measure $P = \{(p_u, A_u)\}$, $A_u > 0$, $\sum_u A_u = \frac{4}{3}\pi$; a threshold ϵ .

Output: The unique discrete OMT-Map $\varphi : \mathbb{D}^3 \rightarrow P$.

Scale and translate P , such that $P \subset \mathbb{D}^3$.

Initialize $h_u \leftarrow -\frac{1}{2} \langle p_u, p_u \rangle$.

repeat

 Compute the upper envelope $\text{Env}(\{\pi_u\})$, where the plane $\pi_u(p) = \langle p_u, p \rangle + h_u$,

 Project the upper envelope to obtain the power diagram $\mathcal{D}(\mathbf{h})$,

 Compute the dual power Delaunay triangulation $\mathcal{T}(\mathbf{h})$,

 Compute the cell volumes $\mathbf{w}(\mathbf{h}) = (w_u(\mathbf{h}))$.

 Compute $\nabla E(\mathbf{h})$ using Eqn. (26).

 Compute the Hessian matrix using Eqn. (27).

 Update the height vector $\mathbf{h} \leftarrow \mathbf{h} - \delta H^{-1} \nabla E(\mathbf{h})$.

until $\|\nabla E\| < \epsilon$.

return $\varphi : \Omega \rightarrow P$, $W_u(\mathbf{h}) \rightarrow p_u$.

mapping from M to the unit solid ball \mathbb{D}^3 . The algorithm pipeline is described in Alg. 4.

Suppose $t \in K$ is a tetrahedron in M , with vertices $\{u, v, w, l\}$. We calculate its volume using the formula:

$$\text{vol}(t) = \frac{1}{6} \begin{vmatrix} x^u & y^u & z^u & 1 \\ x^v & y^v & z^v & 1 \\ x^w & y^w & z^w & 1 \\ x^l & y^l & z^l & 1 \end{vmatrix}.$$

The total volume of M is the summation of the volumes of all tetrahedra,

$$\text{vol}(M) = \sum_{t \in M} \text{vol}(t).$$

Then we scale the whole tetrahedron mesh M , such that the total volume equals to $\frac{4}{3}\pi$.

We use the algorithms described in the previous subsections to find the harmonic map from M to \mathbb{D}^3 , $\mathbf{f} : M \rightarrow \mathbb{D}^3$. For each vertex $u \in M$, we define the measure associated with it as the one fourth the total volume of all tetrahedra adjacent to it,

$$A_u := \frac{1}{4} \sum_{\{u, v, w, l\} \in M} \text{vol}(\{u, v, w, l\}), \quad (28)$$

therefore, the total measure equals to the volume of the unit solid ball,

$$\sum_{u \in M} A_u = \frac{4}{3}\pi.$$

Then we define the discrete point set with measures

$$P = \bigcup_{u \in M} \{(\mathbf{f}(u), A_u)\}. \quad (29)$$

We compute the discrete optimal mass transportation map $\varphi : \mathbb{D}^3 \rightarrow P$, the inverse map φ^{-1} maps each point $p_u \in P$ to the mass center of W_u . The composition $\varphi^{-1} \circ \mathbf{f} : M \rightarrow \mathbb{D}^3$ is the desired volume-preserving parameterization.

Algorithm 4 Volume-preserving Parameterization

Input: A simply connected tetrahedron mesh M with single boundary surface.

Output: A volume-preserving parameterization.

Compute a volume harmonic mapping $\mathbf{f} : M \rightarrow \mathbb{D}^3$.

Compute the discrete measures using Eqn. (28), construct the measured point set using Eqn. (29).

Compute the discrete optimal mass transportation map $\varphi : \mathbb{D}^3 \rightarrow P$,

return $\varphi^{-1} \circ \mathbf{f} : M \rightarrow \mathbb{D}^3$.

5. Experimental results

In this section, we demonstrate the efficiency and efficacy of our method using examples from real world. All the experiments were conducted on a laptop computer of Intel Core i5-4200U CPU, 2.29 GHz with 8 GB memory. All the algorithms are implemented using C++ with visual studio 2013 on windows10 platform. The envelope of hyperplanes, power Voronoi diagram are computed using CGAL [43].

5.1. Volume-preserving parameterization

We have tested our volumetric parameterization on several models, including Michelangelo's King David in Fig. 4, Stanford bunny in Fig. 5, the bimba sculpture in Fig. 5, the buddha model in Fig. 6, the duck model in Fig. 7, the bimba sculpture model in Fig. 8 and the lion cup model in Fig. 9. Frame (a) shows the input solid

4.4. Volume-preserving parameterization

Let M be the simply connected tetrahedral mesh with a single boundary surface, we would like to compute a volume preserving

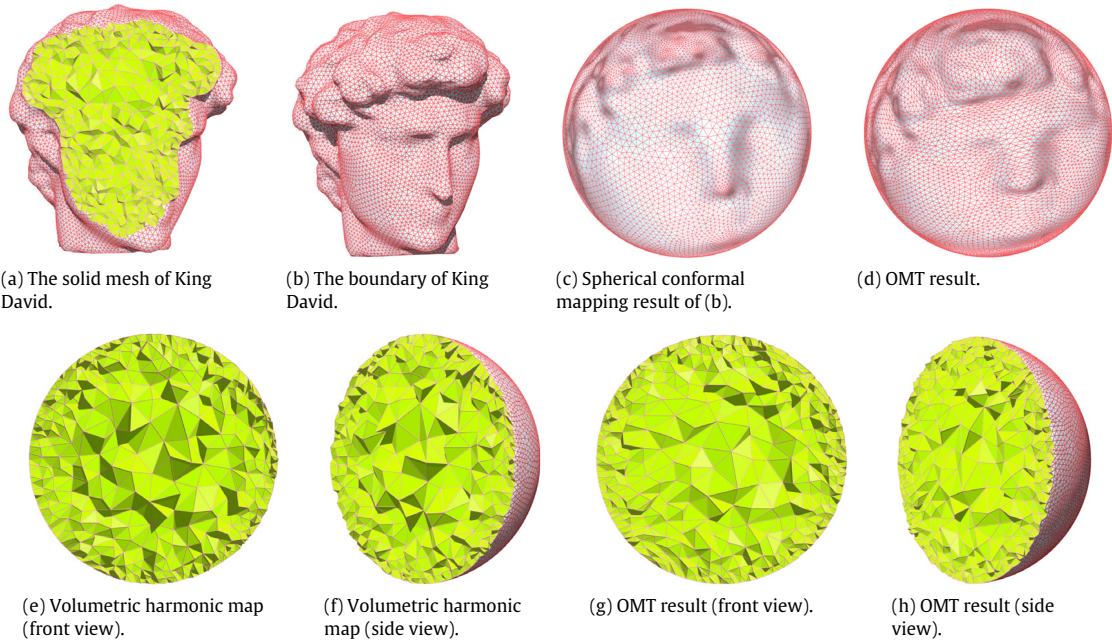


Fig. 4. Volume-preserving parameterization for Michelangelo's King David head model.

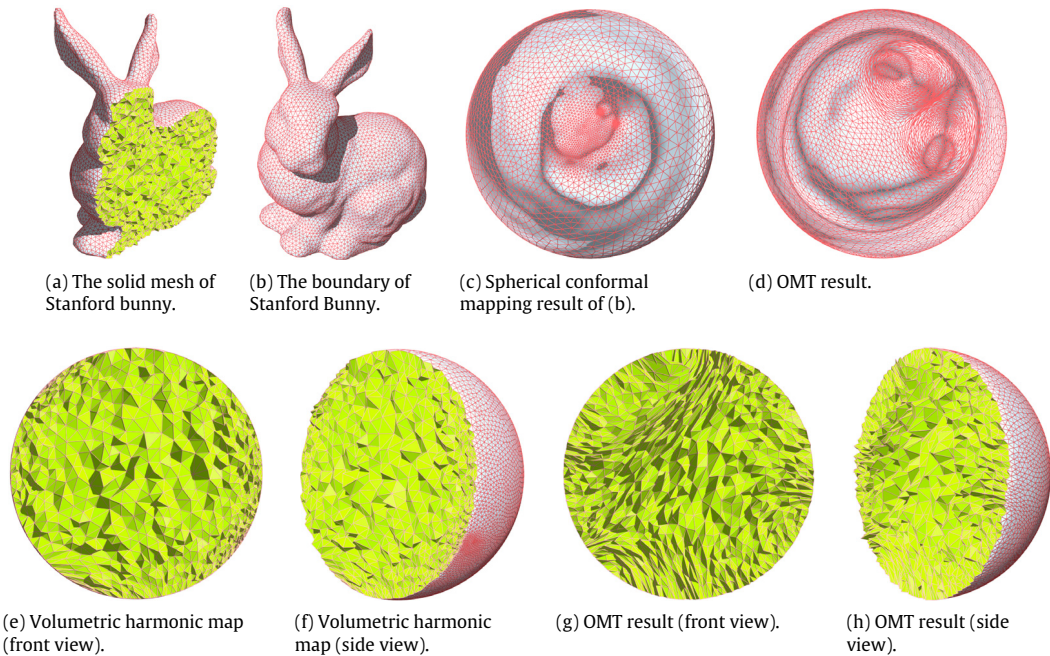


Fig. 5. Volume-preserving parameterization for the Stanford bunny model.

tetrahedron mesh; frame (b) is its 3D boundary surface, frame (c) is the spherical conformal mapping result of the surface (b); frame (d) shows our OMT mapping result (exterior view). We calculate the volumetric harmonic mapping using the Dirichlet boundary condition of frame (b). The volumetric harmonic map result is shown with the interior structure in frame(e) (front view) and frame (f) (side view); the OMT result is shown with the interior structure in frame (g)(front view) and side frame (h)(side view).

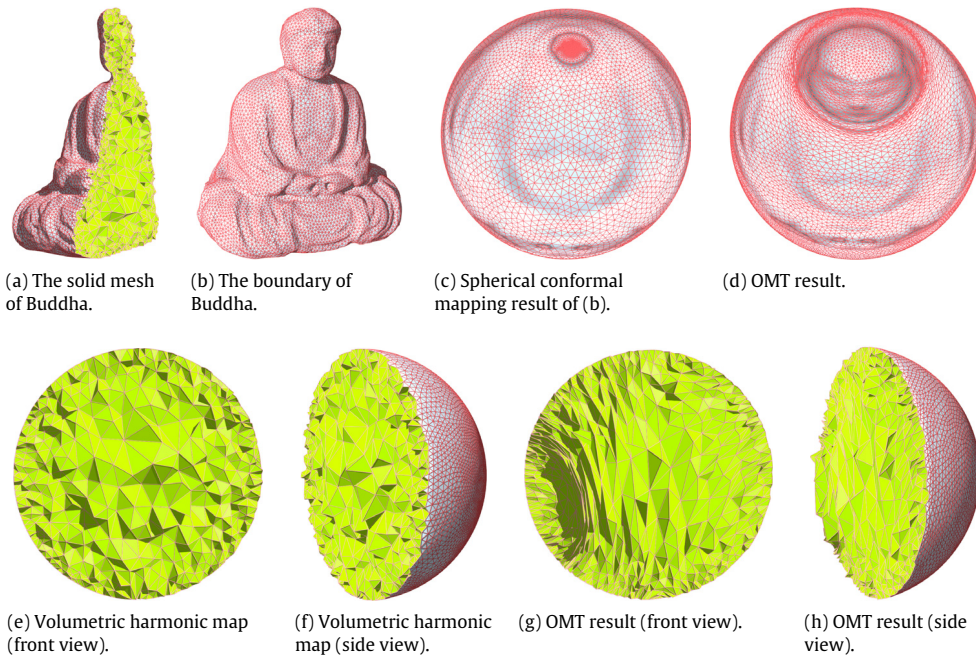
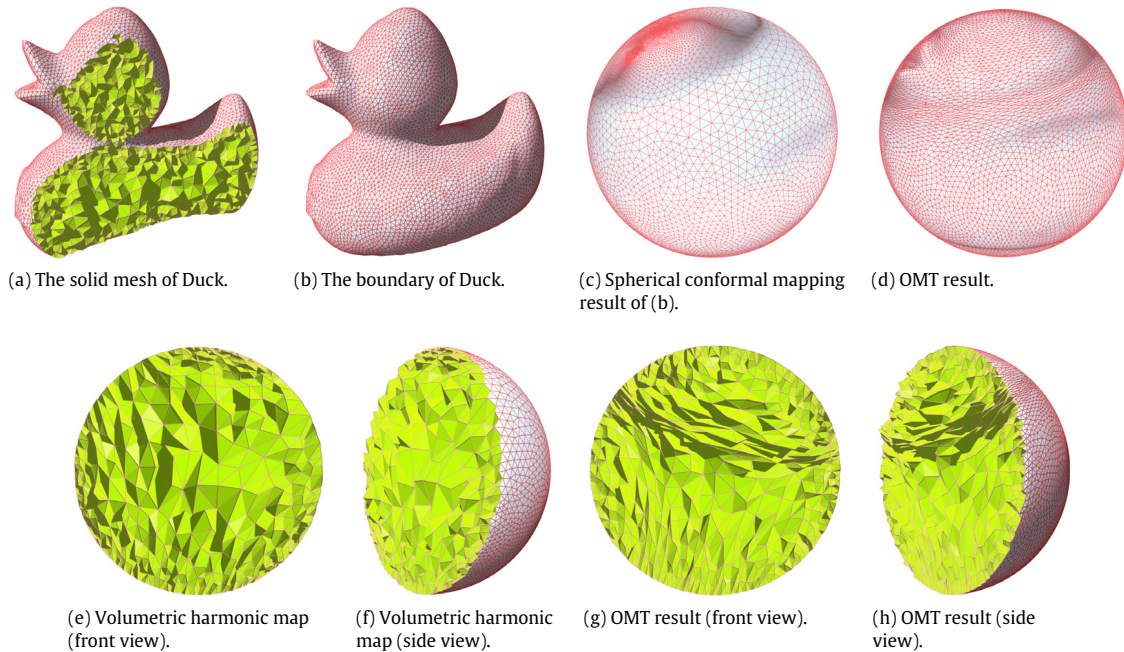
5.2. Volumetric morphing

Volume-preserving parameterization can be directly applied for volumetric morphing. Using volumetric harmonic mapping and OMT technique, we can transform one complex solid model to

the canonical geometry model, the unit solid ball. Figs. 10, 11 show the animation sequence of volumetric morphing, using our volumetric-preserving parameterization technique.

5.3. Comparison

We have compared our volume-preserving parameterization technique with Levy's method [44]. In his work [44], Levy proposes to utilize the uniform sampling and multi-level algorithm to accelerate the computation of OMT. However, Levy's method changes the tetrahedron structure of the input solid, only gives an approximation to OMT and the final result is not bijective on the boundary. In contrast, our method preserves the combinatorial structure

**Fig. 6.** Volume-preserving parameterization for the Buddha model.**Fig. 7.** Volume-preserving parameterization for the Duck model.

of the input solid, gives the accurate solution and the result is bijective for both interior and the boundary surface. Therefore, our method can produce smoother, more physically sensible morphing sequence. By comparing the morphing sequences generated by our method in Figs. 10 and 11 and those by Levy's method in Figs. 12 and 13, we can see Levy's method produces large foldings near the boundary surfaces, whereas our method gives diffeomorphic deformation for the whole solids including the boundaries.

5.4. Quantitative analysis

In order to verify the volume-preserving property of our proposed parameterization algorithms, we calculate the histograms of

angle distortion and volume distortion explicitly. For volume distortion, we compute the ratio between the volume of each tetrahedron in the source solid and the volume of its image in the unit solid ball, and illustrate the histograms of the logarithms of the volume ratios. For angle distortion, we compute the ratio between each dihedral angle in the source solid and that of its image in the parameter domain, and show the histograms of the logarithms of the dihedral angle-ratios.

Figs. 14–16 show the distortion distributions of the King David, Buddha and Duck, respectively. For each model, frame (a) shows the volume-distortion of the volumetric harmonic mapping; frame (b) illustrates the volume-distortion of the volumetric-preserving parameterization; frame (c) the angle-distortion of

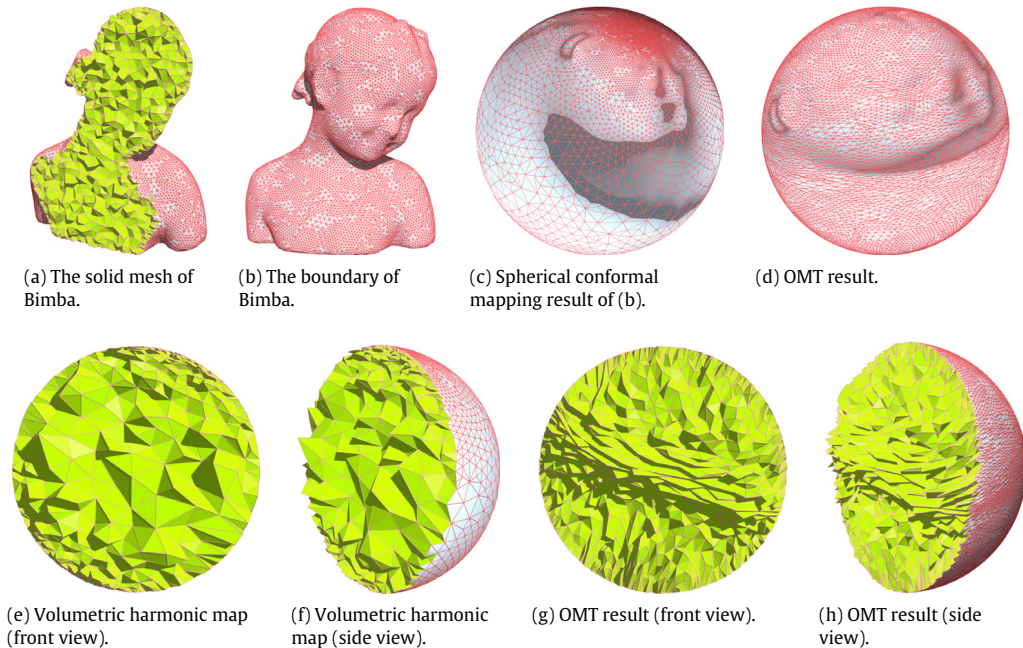


Fig. 8. Volume-preserving parameterization for the Bimba sculpture model.

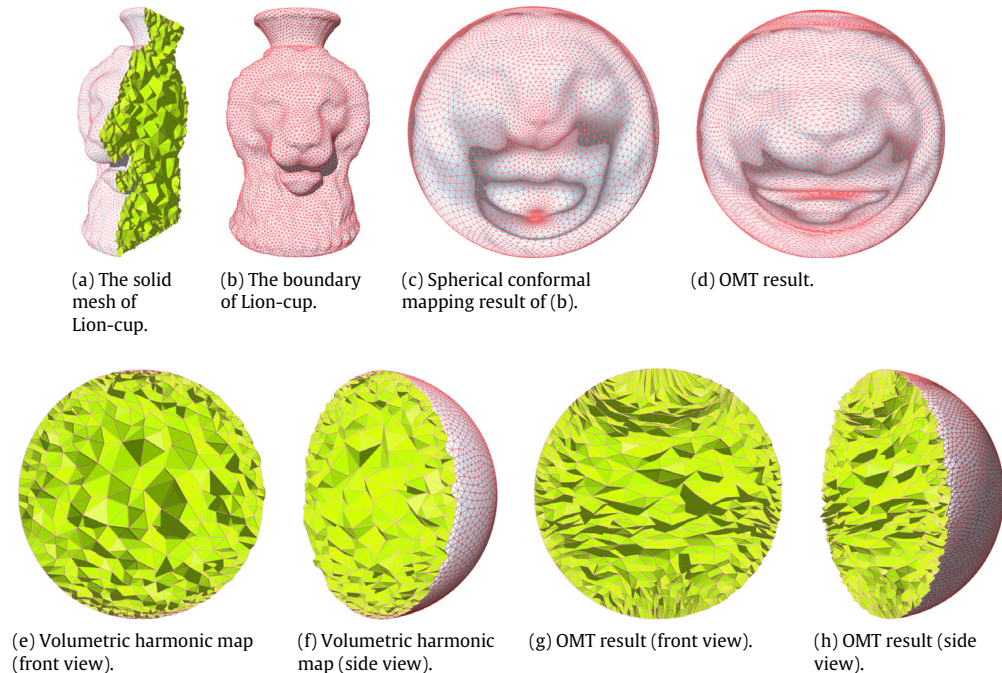


Fig. 9. Volume-preserving parameterization for the Lion-cup model.

the harmonic mapping; frame (d) the angle-distortion of the volumetric-preserving parameterization.

By carefully examining the histograms in frames (a) and (b), one can see that the volume-distortion histograms produced by the volume-preserving parameterization algorithm are highly concentrated near the origin, which verifies that our parameterizations are highly volume-preserving; in contrast, the volume-distortion histograms produced by the volumetric harmonic mappings are much more dispersed. The angle-distortion histograms in frame (c) and (d) show that our volume-distortion parameterization method produces small angle distortions as well. Furthermore, the

experiments validate one merit of our proposed OMT algorithm, the robustness to mesh tessellation. The algorithm performs well even if the input mesh has many very skinny tetrahedra.

Table 1 summarizes the number of iterations and the computation time for different models. Current method doesn't apply any sophisticated optimization, such as multi-level or dynamic kinetics and so on. Unlike the surface harmonic mapping, the volumetric harmonic mapping cannot guarantee the mapping is bijective. In general, there will be small number of flipped tetrahedra, which can be easily fixed manually. We report the number of flipped tetrahedra in the table as well.

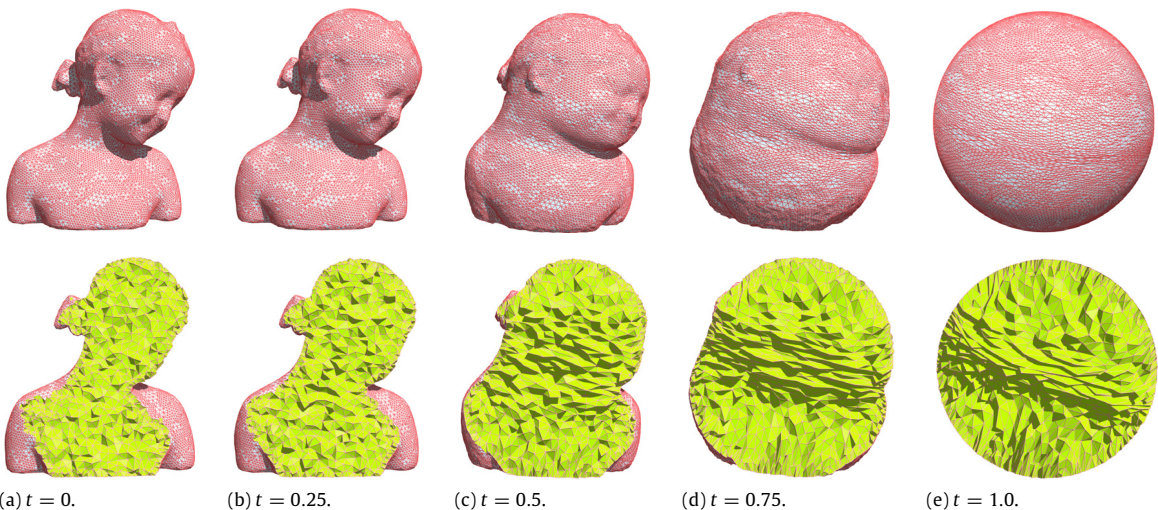


Fig. 10. The volumetric morphing process from the Bimba sculpture to the unit solid ball using our volumetric-preserving parameterization technique.

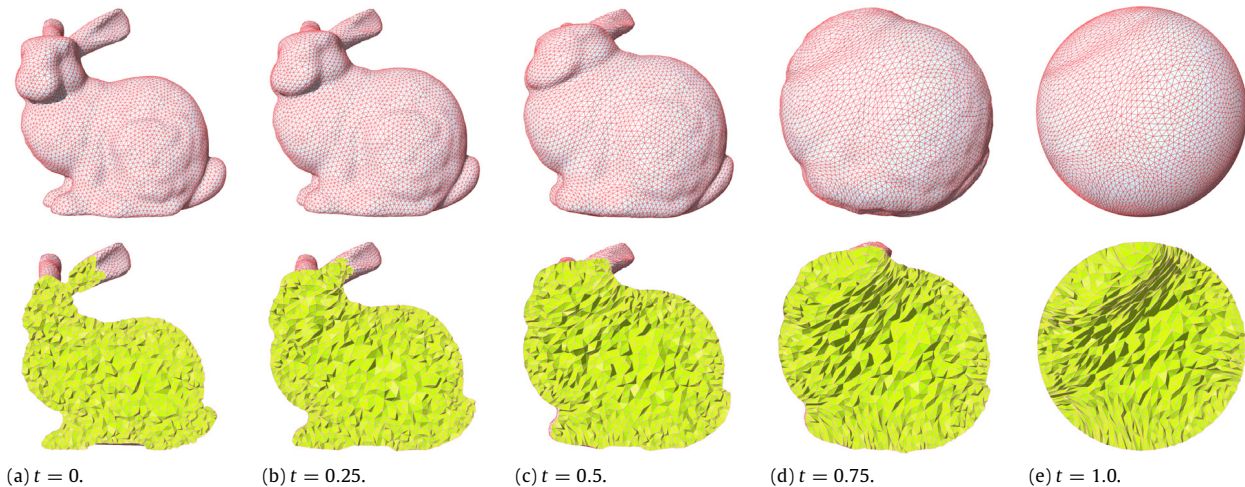


Fig. 11. The volumetric morphing process from the Stanford bunny to the unit solid ball using our volumetric-preserving parameterization technique.

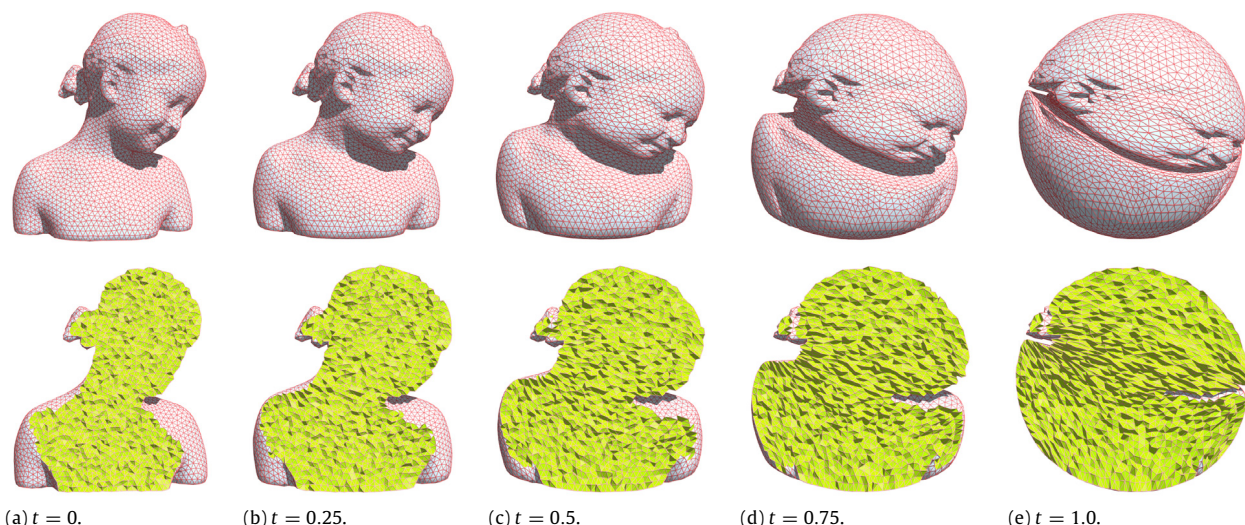


Fig. 12. The volumetric morphing sequence of the Bimba model (front view) using Levy's method.

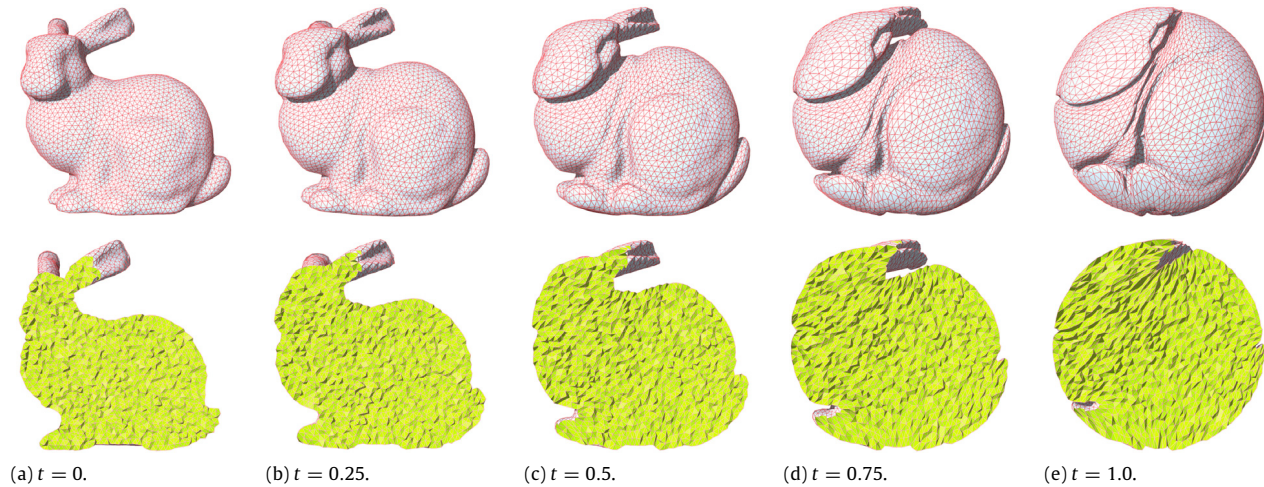


Fig. 13. The volumetric morphing sequence of the Stanford Bunny model (side view) using Levy's method.

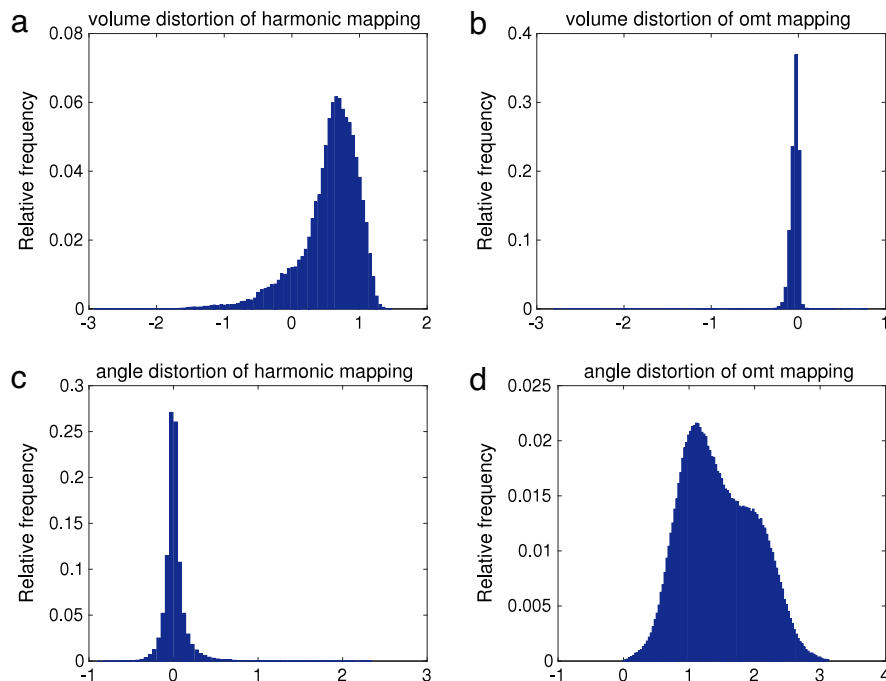


Fig. 14. The comparison histograms of the volume and angle distortion; (a) Volume distortion of harmonic mapping for David King; (b) Volume distortion of OMT for David King; (c) Angle distortion of harmonic mapping for David King; (d) Angle distortion of OMT for David King.

6. Summary and future directions

This work proposes a novel volume-preserving parameterization method for simply connected tetrahedron mesh with a single boundary surface. The method is based on optimal mass transportation theory. The algorithm includes three main steps, boundary surface harmonic mapping, volumetric harmonic mapping, and volumetric optimal mass transportation map.

The method has solid theoretic foundation, utilizes the mature algorithms from computational geometry, produces volumetric parameterizations with the volume-preserving property. We have tested our algorithm on many models in real life, which demonstrates the efficiency and efficacy of the method. To the best of our knowledge, this is the first work addressing volume-preserving parameterization in the literature.

In the current version of implementation, we focus on proving the concepts and no code optimization has been considered. In the future version, we will focus on improving the efficiency

by adopting the hierarchical optimal transportation framework, which will significantly reduce the time complexity.

This work is based on volumetric harmonic map, which may not produce diffeomorphic mapping. In the future, we will explore alternative volumetric mapping algorithms to replace this step and generalize the method to volumes with more complicated topologies. Furthermore, we will apply the proposed method for Spline volume parameterization and Spline volume fitting.

Acknowledgments

We thank the editor and all the anonymous reviewers for their valuable advices and suggestions to improve the quality of the current work. This work was supported by National Natural Science Foundation (Grant Nos. DMS-1418255, DMS-1221339), AFOSR FA9550-10-1-0294, AFOSR FA9550-2614-1-0193, National Natural Science Foundation of China (Grant No. 61328206,

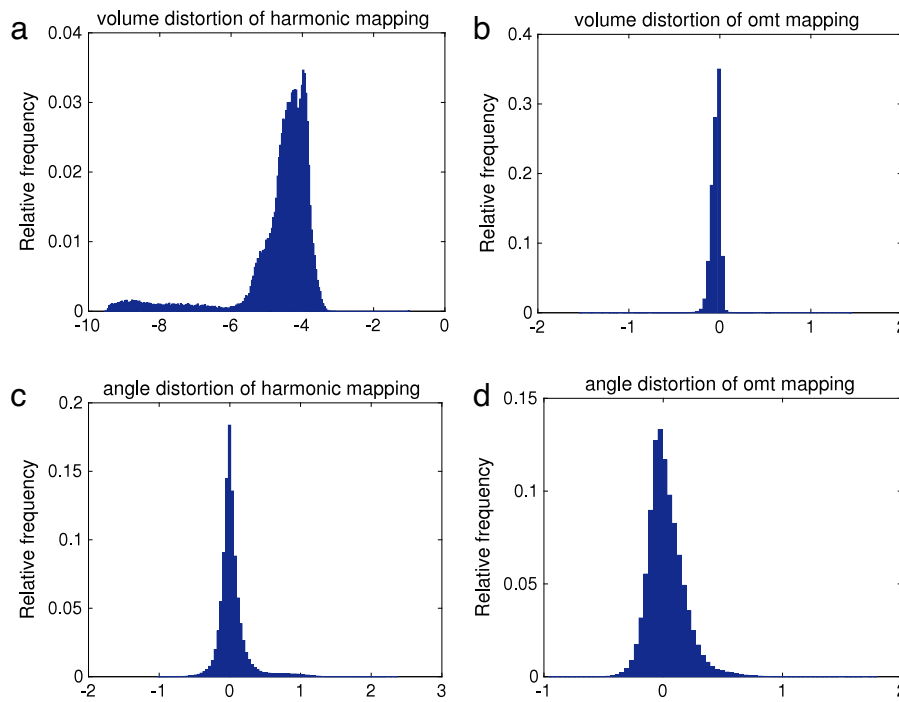


Fig. 15. The comparison histograms of the volume and angle distortion for Buddha model.

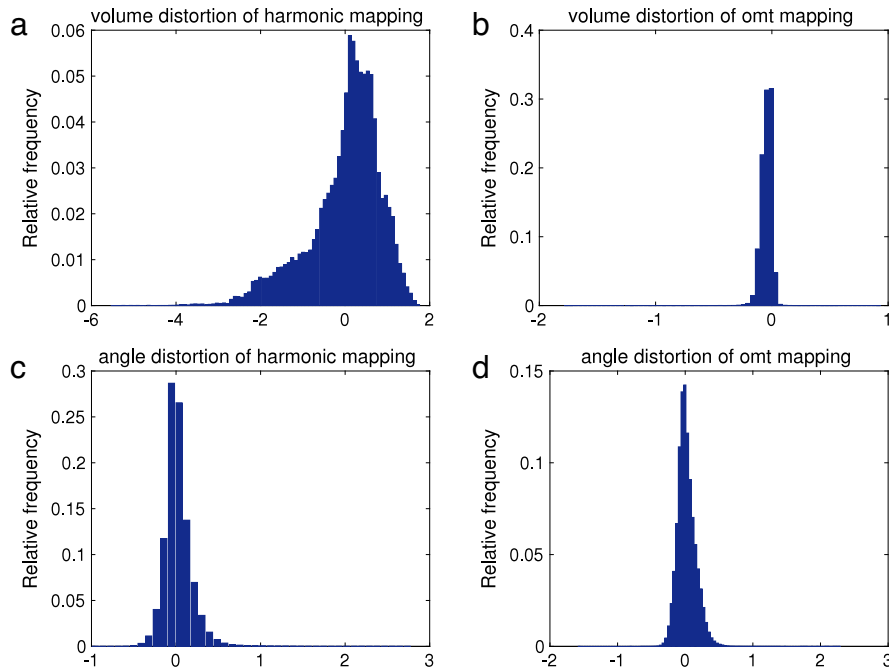


Fig. 16. Comparison histograms of the volume and angle distortion for Duck model.

Table 1
Performance statistics.

Model	Vertices	Tetrahedron	Iteration	Total time (s)	Flip tetrahedrons
David King	19 984	90 576	24	17 758	0
Bunny	22 466	116 740	386	151 084	13
Buddha	20 934	99 113	91	50 480	8
Duck	20 320	96 873	63	31 634	4
Bimba	21 700	89 282	58	35 304	9
Lion-cup	20 874	97 132	50	33 257	4

No. 11271156) and Ph.D. Programs Foundation of Ministry of Education of China (Grant No. 20120141120006).

References

- [1] Hughes TJR, Cottrell J, Bazilevs Y. Isogeometric analysis: Cad, finite elements, nurbs, exact geometry and mesh refinement. *Comput Methods Appl Mech Engrg* 2005;194:4135–95.
- [2] Cottrell J, Hughes T, Bazilevs Y. Isogeometric analysis: toward integration of CAD and FEA. Chichester (UK): Wiley; 2009.
- [3] Varady T, Martin R, Cox J. Reverse engineering of geometric models - an introduction. *Comput-Aided Des* 1997;29(4):255–68.
- [4] Si H. Tetgen, a delaunay-based tetrahedral mesh generator. *ACM Trans Math Softw* 2015;41(2):11:1–11:36.
- [5] Wang Y, Gu X, Yau S-T. Volumetric harmonic map. *Commun Inf Syst* 2004; 3(3):191–202.
- [6] Wang Y, Gu X, Chan TF, Thompson PM, Yau S-T. Brain surface conformal mapping and brain volumetric harmonic map with variational methods, in: SIAM Conference on Imaging Science, Salt Lake City, Utah, 2004.
- [7] Li X, Guo X, Wang H, He Y, Gu X, Qin H. Meshless harmonic volumetric mapping using fundamental solution methods. *IEEE Trans Autom Sci Eng* 2009;6(3): 409–22.
- [8] Xu H, Yu W, Gu S, Li X. Biharmonic volumetric mapping using fundamental solutions. *IEEE Trans Vis Comput Graphics* 2013;19(5):787–98.
- [9] Marin T, Cohan E, Kirby RM. Volumetric parameterization and trivariate b-spline fitting using harmonic function. *Comput Aided Geom Design* 2009; 26(6):648–64.
- [10] Xia J, He Y, Han S, Fu CW, Luo F, Gu X. Parameterization of star-shaped volumes using greens functions. In: Advances in geometric modeling and processing, Vol. 6130. Berlin, Heidelberg: Springer; 2010. p. 219–35.
- [11] Xia J, He Y, Yin X, Han S, Gu X. Direct-product volumetric parameterization of handlebodies via harmonic fields, in: Shape Modeling International, SMI, 2010.
- [12] Gupta V, Voruganti HK, Dasgupta B. Domain mapping for volumetric parameterization using harmonic functions. *Comput-Aided Des Appl* 2014; 11(4):426–35.
- [13] Li XY, Ju T, Hu SM. Cubic mean value coordinates. *ACM Trans Graph* 2013; 32(4):126:1–126:10.
- [14] Floater MS. Mean value coordinates. *Comput Aided Geom Design* 2003;20(1): 19–27.
- [15] Ju T, Schaefer S, Warren J. Mean value coordinates for closed triangular meshes. *ACM Trans Graph* 2005;24(3):561–6.
- [16] Floater GKMS, Reimers M. Mean value coordinates in 3d. *Comput Aided Geom Design* 2005;22(7):623–31.
- [17] Lipman Y, Levin D, Cohen-Or D. Green coordinates. *ACM Trans Graph* 2008; 27(3):78:1–78:10.
- [18] Chao I, Pinkall U, Sanan P, Schröder P. A simple geometric model for elastic deformations. *ACM Trans Graph* 2010;29(4): 38:1–6.
- [19] Nieser M, Reitebuch U, Polthier K. Cube cover parameterization of 3d volumes. *Comput Graph Forum* 2011;30(5):1397–406.
- [20] Huang J, Tong Y, Wei H, Bao H. Boundary aligned smooth 3d cross-frame field. *ACM Trans Graph* 2011;30(6): 143:1–8.
- [21] Li Y, Liu Y, Xu W, Wang W, Guo B. All-hex meshing using singularity-restricted field. *ACM Trans Graph* 2012;31(6):177:1–177:11.
- [22] Jin Y, Qian G-P, Zhao J-Y, Chang J, Tong R-F, Zhang J. Stretch-minimizing volumetric parameterization. *J Comput Sci Tech* 2015;30(3):553–64.
- [23] Bonnotte N. From Knothe's rearrangement to Brenier's optimal transport map, arXiv:1205.1099, 2012, p. 1–29.
- [24] Kantorovich LV. On a problem of Monge. *Uspekhi Mat Nauk* 1948;3:225–6.
- [25] Ruschendorf L. Mass transportation problems, Vol. I-II. New York: Springer; 1998.
- [26] Dominitz A, Tannenbaum A. Texture mapping via optimal mass transport. *TVCG* 2010;16(13):419–32.
- [27] Rehman T, Haber E, Pryor G, Melonakos J, Tannenbaum A. 3D nonrigid registration via optimal mass transport on the GPU. *Med Image Anal* 2009; 13:931–40.
- [28] Brenier Y. Polar factorization and monotone rearrangement of vector-valued functions. *Comm Pure Appl Math* 1991;64:375–417.
- [29] Gu X, Luo F, Sun J, Yau S-T. Variational principles for Minkowski type problems, discrete optimal transport, and discrete Monge-Amperé equations. *Asian J Math (AJM)* 2016;20(2):3830398.
- [30] Su Z, Wang Y, Shi R, Zeng W, Sun J, Luo F, et al. Optimal mass transport for shape matching and comparison. *IEEE Trans Pattern Anal Mach Intell (TPAMI)* 2015;37(11):2246–59.
- [31] Zhao X, Su Z, Gu XD, Kaufman A, Sun J, Gao J, et al. Area-preservation mapping using optimal mass transport. *TVCG* 2013;19(12):2838–47.
- [32] Schoen R, Yau S-T. Lectures on harmonic maps. International Press; 1997.
- [33] Gu X, Yau S-T. Computational conformal geometry. International Press; 2008.
- [34] Villani C. Topics in optimal transportation. Graduate studies in mathematics, No. 58. American Mathematical Soc.; 2003.
- [35] Villani C. Topics in optimal transportation. American Mathematical Society; 2003.
- [36] Berg MD, Kreveld MV, Overmars M, Schwarzkopf OC. Computational geometry. Springer; 2000.
- [37] Alexandrov AD. Convex polyhedra. Springer; 2005.
- [38] Aurenhammer F. Power diagrams: properties, algorithms and applications. *SIAM J Comput* 1987;16:78–96.
- [39] Gu X, Wang Y, Chan TF, Thompson PM, Yau S-T. Genus zero surface conformal mapping and its application to brain surface mapping. *IEEE Trans Med Imaging (TMI)* 2004;23:949–58.
- [40] Xu G, Mourrain B, Duvigneau R, Galligo A. Analysis-suitable volume parameterization of multi-block computational domain in isogeometric applications. *Comput-Aided Des* 2012;45(2):395–404.
- [41] Xu G, Mourrain B, Duvigneau R, Galligo A. Constructing analysis-suitable parameterization of computational domain from cad boundary by variational harmonic method. *J Comput Phys* 2013;252:275–89.
- [42] Wang X, Qian X. An optimization approach for constructing trivariate b-spline solids. *Comput-Aided Des* 2014;46:179–91.
- [43] Project TC. CGAL User and Reference Manual, CGAL Editorial Board, 2015. URL <http://doc.cgal.org/4.7/Manual/packages.html>.
- [44] Lévy B. A numerical algorithm for l^2 semi-discrete optimal transport in 3d. *ESAIM Math Model Numer Anal* 2015;49(6):1693–715.